Yu *et al. Journal of Wood Science* (2022) 68:29
https://doi.org/10.1186/s10086-022-02036-3

Journal of Wood Science

ORIGINAL ARTICLE Open Access

Preparation of carbon nanoparticles from activated carbon by aqueous counter collision

Liwei Yu, Daisuke Tatsumi and Tetsuo Kondo*

Abstract

In the present study, crystalline cellulose biomass material was converted into carbon nanoparticles via carbonization to activated carbon with micropores of various sizes. This was subsequently subjected to aqueous counter collision (ACC) to produce hydrophobic porous functional particles. Initially, raw crystalline cellulose material was carbonized into activated carbon materials with various pore distributions prior to ACC. Pore distribution depended on the activation time, and was confirmed by nitrogen (N_2) adsorption isotherms. The surface areas and pore volumes of carbon activated for 8 h were larger than those of carbon activated for 2 h. When they were subjected to ACC, the width and length of the carbon particles decreased as the number of pulverizing cycles during the ACC treatment increased. Eventually, carbon nanoparticles of 70 nm width that had improved dispersibility and stability were produced. The diameters of the carbon nanoparticles and their dispersibility were dependent on the pore distribution and surface areas of the activated carbon subjected to the ACC treatment. The ACC process facilitated the preparation of carbon nanoparticles from activated carbon derived from biomass, and is, therefore, an important strategy for the sustainable production of a sought-after and valuable resource.

Keywords: Carbon nanoparticle, Aqueous counter collision, Dispersibility, Activated carbon, Pore distribution

Introduction

Nanocarbons have recently attracted considerable attention, because they are light-weight and have high specific surface areas and favorable electrical and mechanical properties. Interest was roused in the 1980s with the discovery of fullerenes by Kroto et al. [1–3], followed by carbon nanotubes (CNTs) [4], and graphene [5]. These materials have promising properties that can be used in various applications. For example, the electrical properties of CNTs have been exploited in nanowires [6, 7], field-effect transistors [8], and nanoscale electronic devices [9–11]. Owing to their high Young's moduli and aspect ratios, CNTs can also be used to make high-strength fibers [12, 13]. Graphene also has many fascinating properties, such as high charge carrier mobility, and chemical and mechanical stability. Therefore, it has been used in a wide variety of applications, including energy storage, polymer composites, and bio- and chemical sensors [14–17].

Recently, diverse synthetic strategies such as chemical and electro-chemical exfoliation [18, 19] and chemical vapor deposition (CVD) [20–22] have been developed to prepare carbon nanoparticles. Graphene can be produced by transversely cutting carbon nanofibers (CNFs) via chemical exfoliation [23]. However, the nanocarbon yield is comparatively low, which raises its price. Moreover, it is difficult to prepare carbon nanoparticles via a top-down procedure without using chemical agents. Therefore, in consideration of the points mentioned above, in the present article we propose a facile method for converting crystalline cellulose biomass into carbon nanoparticles through activated carbon.

*Correspondence: tekondo@agr.kyushu-u.ac.jp

Graduate School of Bioresource and Bioenvironmental Sciences, Kyushu University, Motooka 744, Nishi-ku, Fukuoka 819-0395, Japan

Activated carbon comprises a random network of nanometer-sized fragments of graphite (nanocarbon domains), in which each domain forms a stack of three or four nanosized graphene. The individual nanocarbon domains are loosely packed by weak interactions, such as van der Waals forces, and the structure consists of numerous nanometer-sized pores (micropores) [24–26]. Activated carbon is usually prepared by one of two methods: either physical or chemical activation. Phosphoric acid has often been used to activate lignocellulosic materials, because that route has environmental benefits and produces high yields [27, 28]. Zuo et al. [29] showed that the duration of impregnation and the nature of the parent lignocellulosic material affect the porosity during phosphoric acid activation. In a previous study [30], we investigated the effect of phosphoric acid activation at high temperatures on the graphitic microcrystal growth of wood-based chars. We found that phosphorus-containing groups promote the growth of graphitic microcrystalline domains, which enables the formation of graphite. The pore structure of the activated carbon is produced when the nanocarbon domains, which are held together by weak interactions, are peeled apart.

Previously, aqueous counter collision (ACC), which is a top-down technique, has dealt with activated carbon particles, such as CNTs and graphene by downsizing them on a nano-scale [31]. ACC is capable of solely cleaving the intermolecular interactions in biomass materials [32–35] as well as carbons [31]. The technique uses dual water jets to downsize the carbon particles into nano-objects without the necessity of chemical modification—including the depolymerization of molecules. During ACC, aqueous suspensions containing micro-sized particles are directed at each other at high speed so that the particles collide. This generates elastic–plastic waves that convert the particles into nano-scaled objects, thereby dispersing them in water. It is possible to obtain nanoscale objects of the desired size by controlling the repetition of the collision and the ejection pressure of the water jets [33–35].

In the present study, starting with crystalline cellulose biomass, carbon nanoparticles were successfully prepared via carbonization to activated carbon and subsequent ACC. The ACC process produced activated carbon with micropores of various sizes. Subsequently, the dependence of the pore characteristics in the activated carbon on the carbon nanoparticle suspension was investigated, and the obtained carbon nanoparticles were characterized.

Materials and methods

Carbonization of cellulose samples

A sample of tunics of *Halocynthia* sp. [33] was used as a starting material, because it contains high crystalline (86%) cellulose. The sample was homogenized using a food processor and purified by treating in aqueous 5% potassium hydroxide solution at 80 °C for 3 h and was stood at room temperature for 12 h. It was then neutralized in 0.1 N hydrochloric acid and washed well with distilled water. The purified tunicate cellulose (TC) was freeze-dried before usage. The TC samples were pyrolyzed in a TMF-500 N tube furnace (AS ONE Co., Ltd., Osaka, Japan) under a nitrogen flow. The samples were pyrolyzed by heating them to 800 °C at a rate of 5 °C/min, and maintaining that temperature for 1 h. This is a non-activated (i.e., 0-h-activated) TC carbon, which was used as a control.

Acid pretreatment for activation

The obtained TC carbons were ground into particles (0.2–0.5 mm in diameter). The particles (0.25 g) were then impregnated with 50 mL of 20% phosphoric acid (H_3PO_4) solution. The mixture was kept in a water bath at 80 °C for 2 or 8 h, which were defined as 2- or 8-h-activated, respectively. Each of them was placed in a ceramic boat container (14 mm wide; 12 mm high; 140 mm long). The container was then placed in the middle of the furnace, the tube of which was 50 mm in diameter and 500 mm long. For activation, the tube was first purged with nitrogen (N_2) at a flow rate of approximately 200 mL/min. The impregnated material was then heated from room temperature to 800 °C at a rate of 5 °C/min, and held at that temperature for 60 min. The N_2 flow rate of 50 mL/min was maintained throughout the entire activation, including the stage in which the samples were cooled back down to room temperature. Both the 2-h- and 8-h-activated TC carbons were filtered by washing repeatedly with warm deionized water until phosphorus was undetectable.

Pore characteristics of the activated carbons

Information on the pore structure of the activated TC carbons was estimated using gas adsorption and small angle X-ray scattering (SAXS) measurements. The adsorption of N_2 as a probe species was performed at −196 °C using a BEL SORP18 system (BEL JAPAN Co., Ltd., Osaka, Japan). The nitrogen adsorption isotherms of the activated carbon samples were acquired over the relative pressure (P/P_0) range 0–1. Before obtaining the adsorption isotherms, the activated carbons were heated to 200 °C for 5 h in a vacuum to clean their surfaces. The specific surface area (S_{BET}) values and micropore volume (V_{mic}) values of the samples were estimated from Brunauer–Emmett–Teller (BET) analysis [36], and the subtracting pore effect method [37] using an α_s-plot. The total pore volume (V_{tot}) was calculated from the amount of nitrogen adsorbed at a relative pressure of

0.99. The volume of transitional pore, which is described as mesopore volume (V_{mes}), was obtained by subtracting V_{mic} from V_{tot}. The pore size distribution was estimated from the nitrogen adsorption isotherms.

The SAXS measurements were performed using synchrotron radiation at the BL-11 beam line of the SAGA Light Source, with the approval of the Kyushu Synchrotron Light Research Center, Tosu, Japan. The beam energy (E) was 8.0 keV and the camera length was 2.641 m. The closed pore structure of the activated carbons was determined from the SAXS profiles.

ACC treatment of activated TC carbons

ACC was carried out according to the method described in the literature [31–33]. The sample suspensions in the sample tank were divided between the dual nozzles, then pressurized and accelerated using a plunger. They collided with each other at high velocity, resulting in wet and rapid pulverization into nano-scaled objects dispersed in water [31–35].

In the present study, 0.1 g of the activated TC carbon was dispersed in 800 mL of pure water for the ACC treatment. The aqueous suspension in the sample tank was then ejected from a pair of nozzles at 160 MPa in 0, 30, or 60 cycles (passes). ACC-treated carbon particles were produced for investigation with a transmission electron microscope (TEM).

Transmission electron microscopy

The sizes of the ACC-treated carbon particles were determined from images obtained using a JEM-1010 TEM (JEOL, Ltd., Tokyo, Japan). The sample suspension (0.012%) was dropped onto a copper grid and freeze-dried for 20 min before examination using the TEM at an accelerating voltage of 80 kV. The acquired images were scanned for digitization to determine the widths and lengths of the carbon nanoparticles. Contrast enhancement, calibration of scale, statistical size data collection, and cross section along a desired line were carried out on the images using Image Pro Plus software v.4.1 (Media Cybernetics Co., Ltd., Tokyo, Japan). Both width and length were measured for more than 50 specimens in the same pass sample.

Crystallographic properties

Wide-angle X-ray diffraction (WAXD) patterns of the samples were obtained using a RINT2100V system (Rigaku Co., Tokyo, Japan) at 20 mA and 40 kV. Diffraction intensities were collected in the range $2\theta = 5–40°$.

Elemental analysis by X-ray fluorescence measurements

X-ray fluorescence spectra were obtained using a wavelength dispersive spectrometer (EDX-7000, Shimadzu Co., Kyoto, Japan). The measurements were performed at room temperature in a helium atmosphere.

Results and discussion

Crystalline and pore characteristics of the activated TC carbons

The WAXD intensity curves of three samples, i.e., non-activated carbons, 2-h-, and 8-h-activated carbons, before ACC are shown in Fig. 1. The non-activated carbons exhibited a typical amorphous phase. In contrast, the 8-h-activated carbons, which were subjected to a longer impregnation time, had higher crystallinity, because a diffraction peak due to (002) plane of graphite became sharp and was shifted to higher 2θ. This indicates that phosphoric acid promoted the growth of microcrystalline structure during the activation process, so the crystallinity increased as the impregnation time increased. The lattice spacing obtained from the diffraction line (002), d_{002}, was 0.37 nm. Other noises may be due to crystalline "impurity". They could be attributed to phosphate salts remaining in the carbons, because the results of X-ray fluorescence measurements for the carbons indicated that the phosphorus element was the major one except carbon. It was contained at 4.2 wt% in the 8-h-activated carbons. Cations, which are counterions of phosphate, were mainly calcium. Calcium phosphate is known to have a polymorphic crystalline structure, so that many peaks appear in the X-ray diffraction profile.

The temperature and duration of the pretreatment by H_3PO_4 impregnation appeared to be critical factors in controlling the pore structure of the resulting carbons [38]. Figure 2 shows the nitrogen adsorption–desorption isotherms obtained for the phosphoric acid-activated carbons prepared using various impregnation periods. The shapes of the N_2 adsorption isotherms of the two

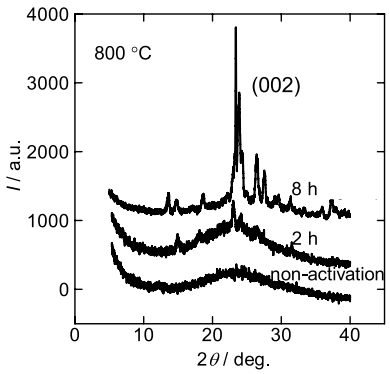

Fig. 1 Wide-angle X-ray diffraction (WAXD) intensity, *I*, profiles of non-activated carbon, and 2-h- and 8-h-activated carbons before aqueous counter collision (ACC)

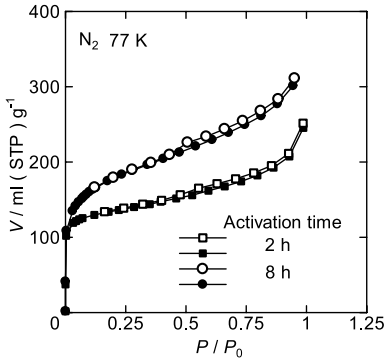

Fig. 2 Adsorption isotherms of 2-h-activated tunicate cellulose (TC) carbon and 8-h-activated TC carbon. The open and closed symbols indicate the desorption and adsorption curves, respectively. *V*/mL (STP) g^{-1} indicates the absorption amount per 1 g of sample. P/P_0 is relative pressure

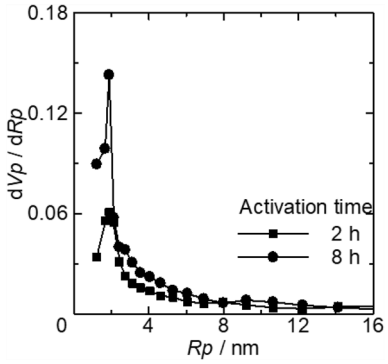

Fig. 3 Pore distribution curves for mesopores of activated tunicate cellulose (TC) carbons. V_p and R_p indicate pore volume and pore size, respectively

Table 1 Pore characteristics of activated tunicate cellulose (TC) carbons prepared by impregnation with a 20% H_3PO_4 solution for various times

Before/ After ACC	Impregnating time/hour	S_{BET}/m^2g^{-1}	V_{tot}/cm^3g^{-1}	V_{mic}/cm^3g^{-1}
Before	2	512	0.40	0.19
	8	659	0.56	0.27
After	2	440	0.43	0.13
	8	694	0.79	0.27

S_{BET}/m^2g^{-1} Brunauer–Emmett–Teller (BET) surface area, V_{mic} micropore volume, V_{tot} total pore volume

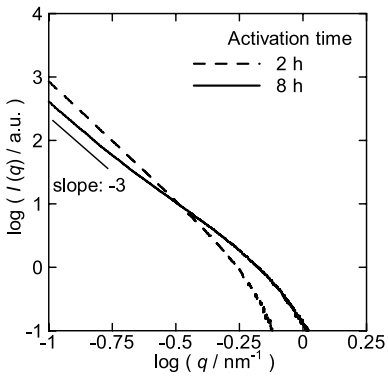

Fig. 4 Small angle X-ray scattering (SAXS) profiles of activated tunicate cellulose (TC) carbons prepared using various impregnation times. *I*(*q*) and *q* indicate scattering intensity and the absolute value of scattering vector

specimens were similar and comprised a mixture of types I and IV based on the IUPAC classification [39]. This indicated that the carbons had mainly micro- and mesoporous characteristics. The quantity of N_2 adsorption onto the activated carbons increased with the duration of H_3PO_4 impregnation, especially in the relatively high-pressure range. The adsorption isotherms were also transformed into BET surface area (S_{BET}/m^2g^{-1}), micropore volume (V_{mic}), and total pore volume (V_{tot}) values, as shown in Table 1. The surface area and pore volume of the 8-h-activated TC carbon were larger than those of the 2-h-activated carbon, indicating that the duration of impregnation should be taken into account to ensure sufficient exposure of the interior of the TC carbon to H_3PO_4.

The mesopore (2–50 nm) distributions were calculated using the Barrett–Joyner–Halenda (BJH) method [40]. As shown in Fig. 3, the pore volumes (V_p) of the mesopores in the 8-h-activated carbon were larger than those of the 2-h-activated carbon. SAXS measurements were used to estimate the closed pore structure of the activated carbons. Figure 4 shows the SAXS profiles of the activated carbons. $I(q)$ is the scattering intensity and q is the absolute value of the scattering vector. In the high q range, a difference appeared in the scattering curves of the activated carbons of various impregnation times. The pore size (d) of the activated carbon was calculated using the expression: $d = 2\pi/q$.

As a result, the SAXS profiles demonstrated that the 8-h-activated carbon had more pores than the 2-h-activated carbon in the q range $10^{-0.5}$–10^{0} nm^{-1}, which corresponds to the pore size range 6–20 nm. This tendency is consistent with the results described above for open pore distribution curves.

Carbon nanoparticles prepared from activated carbon by ACC

The TEM images of the 2-h- and 8-h-activated carbon dispersions prepared by ACC are shown in Fig. 5. The images clearly show that the carbon particles were

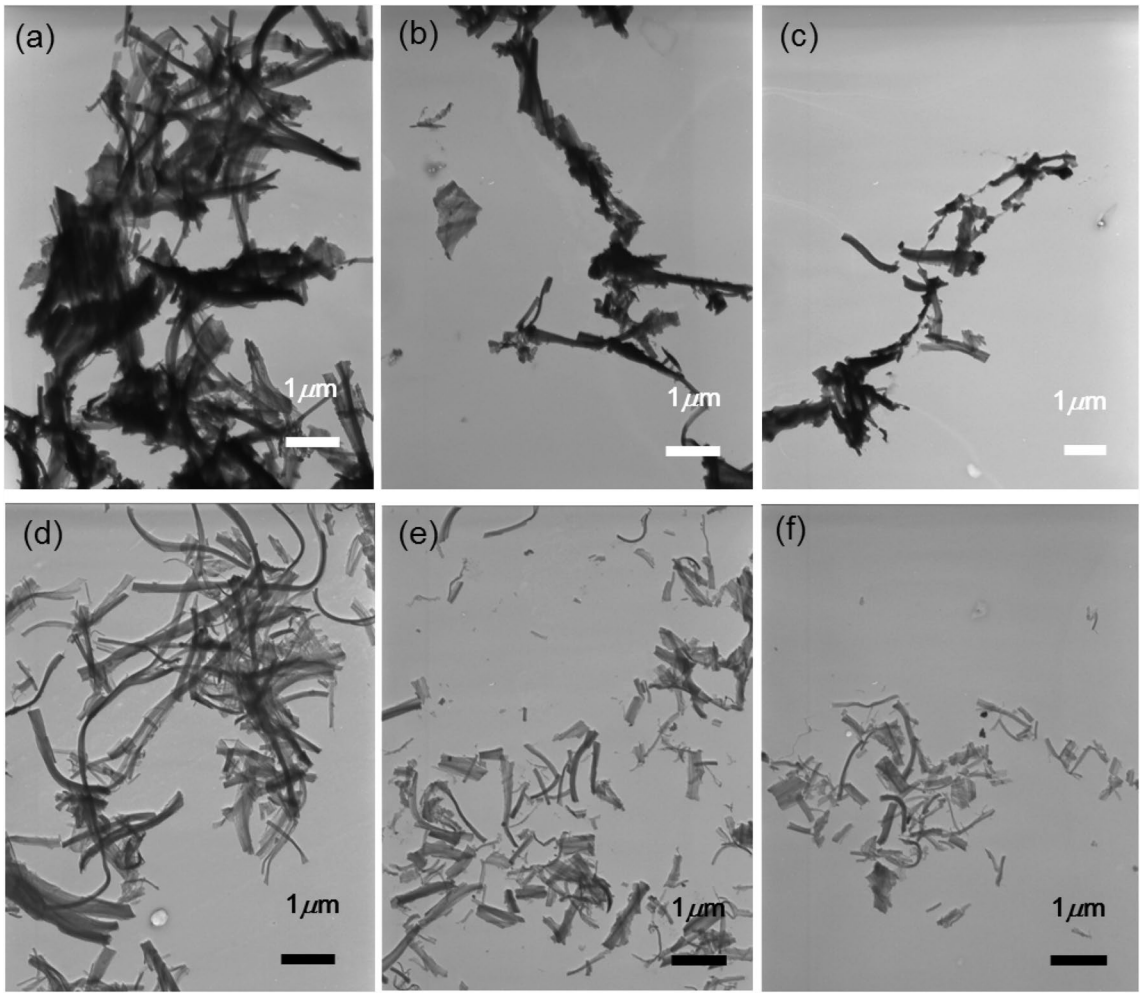

Fig. 5 Transmission electron microscope (TEM) images of 2-h-activated carbon dispersions prepared by aqueous counter collision (ACC) with **a** 0, **b** 30, and **c** 60 passes; and 8-h-activated carbon dispersions prepared by ACC with **d** 0, **e** 30, and **f** 60 passes

mostly strand-shaped. The widths and lengths of the carbon particles decreased as the number of pulverizing cycles (passes) increased (Table 2). Eventually, ACC produced carbon nanoparticles that were 70 nm wide from the 8-h-activated carbon suspension. Throughout the pass range, the 2-h-activated carbon particles were larger than the 8-h-activated particles after ACC.

Figure 6 shows the nitrogen adsorption–desorption isotherms of the 2-h- and 8-h-activated carbons after ACC. The shapes of the isotherms of both the ACC-treated carbons were similar to those of the carbons before ACC (see Fig. 2). This indicates that the amount of N_2 adsorbed on the 8-h-activated carbon was still larger than that adsorbed on the 2-h-activated carbon, even though the particle size had been reduced to the

Table 2 Averaged lengths and widths of the aqueous counter collision (ACC)-treated activated carbon particles

Activation	ACC Pass					
	0		30		60	
	length/nm	width/nm	length/nm	width/nm	length/nm	width/nm
2 h	3290	1243	1918	402	1731	223
8 h	2662	776	916	202	527	70

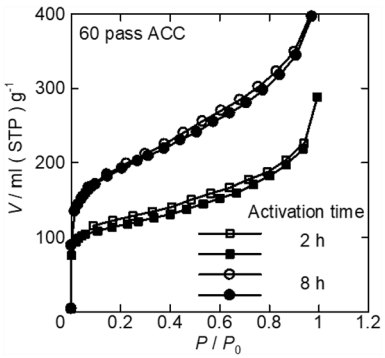

Fig. 6 Adsorption isotherms of 2-h- and 8-h-activated carbons after aqueous counter collision (ACC). Legends are the same as Fig. 2

nanoscale. Considering the data in Table 1, the surface areas of the 2-h-activated carbon particles appeared slightly smaller after ACC than before the treatment. In contrast, the surface areas of the 8-h-activated carbon particles were larger after ACC than before it. It can also be confirmed that the V/mL (STP) g^{-1} for 8-h-activated carbon in Fig. 2 are entirely larger than that in Fig. 6. Presumably, this was because the surfaces of the closed pores in the 8-h-activated particles were larger than those in the 2-h-activated particles. In the case of the 8-h-activated particles, the closed pores were possibly fractured by ACC, which exposed the interior surfaces, and thus the surface areas of the resulting particles increased. As a result, the BET surface areas and pore volumes of the 8-h-activated carbon particles increased after ACC.

After suspended in water, the 8-h-activated TC carbons were precipitated immediately, whereas the 2-h-activated carbons had relatively better dispersibility in water. Furthermore, an aqueous dispersion containing both the 2-h- and 8-h-activated TC carbons was phase-separated within 1 week. This indicated that the two samples had different microstructures prior to ACC.

Because the crystalline density of graphite (~ 2.25 g cm^{-3}) is larger than that of the amorphous phase of activated carbon (0.3–0.6 g cm^{-3}) [41], the amorphous phase may be more favorable for dispersal. Following ACC treatment, the aqueous suspension of the 8-h-activated carbon exhibited improved dispersibility and stability, as evidenced by the absence of phase separation (Fig. 7). This indicates that the greater surface areas of the activated carbons produced by ACC nanopulverization improved their dispersibility in water. Namely, ACC possibly facilitated to produce aqueous suspension of carbon nanoparticles.

Conclusions

In the present study, crystalline cellulose biomass was converted into carbon nanoparticles via carbonization to activated carbon with micropores of various sizes. The activated carbon was subsequently subjected to ACC to produce hydrophobic porous functional particles. The ACC method rapidly produced carbon nanoparticles from micro-sized activated carbon using only high-speed water jets. The carbon nanoparticles in the 8-h-activated carbon were approximately 70 nm in diameter, and formed stable dispersions in water, even after 1 week. The present method can be an advanced process to produce aqueous suspension of carbon nanoparticles.

With regard to the characteristics of the pores in the initial activated carbon, the larger pore volumes and specific surface areas of the activated carbons were more beneficial to the yield of carbon nanoparticles during ACC. This suggests that pore-size-controlled carbon nanoparticles can be prepared by ACC when the pore characteristics are designed for the initial activated

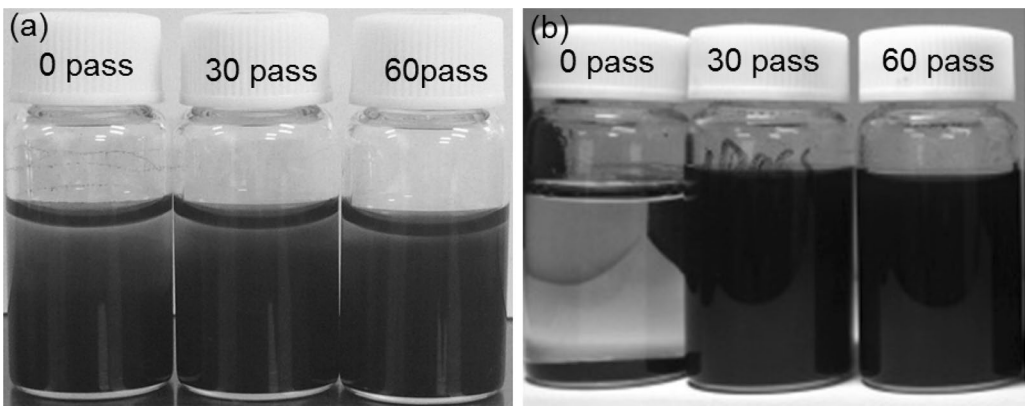

Fig. 7 Photographs of the 2-h- **a** and 8-h- **b** activated carbon dispersions prepared by aqueous counter collision (ACC) with 0, 30, and 60 passes, and left for 1 week

carbon. In other words, the process using ACC facilitates the preparation of water-dispersing nanocarbons, which can open a pathway for a novel strategy of biomass usage.

Abbreviations
ACC: Aqueous counter collision; BET: Brunauer–Emmett–Teller; CNFs: Carbon nanofibers; CNTs: Carbon nanotubes; CVD: Chemical vapor deposition; SAXS: Small-angle X-ray scattering; TC: Tunicate cellulose; TEM: Transmission electron microscope; WAXD: Wide-angle X-ray diffraction.

Acknowledgements
We express special thanks to the late Ryohei Asakura (PhD) from the Fukuoka Industrial Technology Center for his kind support and advice on the adsorption experiments. We also wish to thank professor Shinichiro Wada, Kyushu University, for allowing us to use the X-ray diffractometer.

Author contributions
LY performed all the experiments and prepared the paper. DT was responsible for the research plan, the SAXS and X-ray fluorescence measurements, and for preparation of the paper. TK was responsible for the research plan through study and preparation of the paper. All authors read and approved the final manuscript.

Funding
Not applicable.

Availability of data and materials
Not applicable.

Declarations

Competing interests
The authors declare that they have no competing interests.

Received: 8 December 2021 Accepted: 25 April 2022
Published online: 19 May 2022

References

1. Kroto HW, Heath JR, O'Brien SC, Curl RF, Smalley RE (1985) C60: Buckminsterfullerene. Nature 318:162–163
2. Iijima S (1980) Direct observation of the tetrahedral bonding in graphitized carbon black by high resolution electron microscopy. J Cryst Growth 50:675–683
3. Rohlfing EA, Cox DM, Kaldor A (1984) Production and characterization of supersonic carbon cluster beams. J Chem Phys 81:3322–3330
4. Iijima S (1991) Helical microtubules of graphitic carbon. Nature 354:56–58
5. Novoselov KS, Geim AK, Morozov SV, Jiang D, Zhangs Y, Dubonosi V, Grigorievaand V, Firsov AA (2004) Electric field effect in atomically thin carbon films. Science 306:666–669
6. Dresselhaus MS, Dresselhaus G, Pimenta M (1999) The remarkable properties of carbon nanotubes as nanoclusters. Eur Phys J D 9:69–75
7. Cui Y, Wei Q, Park H, Lieber CM (2001) Nanowire nanosensors for highly sensitive and selective detection of biological and chemical species. Science 293:1289–1292
8. Tans SJ, Verschueren ARM, Dekker C (1998) Room-temperature transistor based on a single carbon nanotube. Nature 393:49–52
9. Tsukagoshi K, Yoneya N, Uryu S, Aoyagi Y, Kanda A, Ootuka Y, Alphenaar BW (2002) Carbon nanotube devices for nanoelectronics. Physica B Condens Matter 323:107–114
10. Franklin NR, Wang Q, Tombler TW, Javey A, Shim M, Dai H (2002) Integration of suspended carbon nanotube arrays into electronic devices and electromechanical systems. Appl Phys Lett 81:913–915
11. Baughman RH, Zakhidov AA, de Heer WA (2002) Carbon nanotubes—the route toward applications. Science 297:787–792
12. Vigolo B, Pe´nicaud A, Coulon C, Sauder C, Pailler R, Journet C, Bernier P, Poulin P (2000) Macroscopic fibers and ribbons of oriented carbon nanotubes. Science 290:1331–1334
13. Dalton AB, Collins S, Muñoz E, Razal JM, Ebron VH, Ferraris JP, Coleman JN, Kim BG, Baughman RH (2003) Super-tough carbon-nanotube fibres. Nature 423:703
14. Gómez-Navarro C, Weitz RT, Bittner AM, Scolari M, Mews A, Burghard M, Kern K (2007) Electronic transport properties of individual chemically reduced graphene oxide sheets. Nano Lett 7:3499–3503
15. Luo J, Tian P, Pan CT, Robertson AW, Warner JH, Hill EW, Briggs GAD (2011) Ultralow secondary electron emission of grapheme. ACS Nano 5:1047–1055
16. Wu Q, Xu Y, Yao Z, Liu A, Shi G (2010) Supercapacitors based on flexible graphene/polyaniline nanofiber composite films. ACS Nano 4:1963–1970
17. Liu Z, Robinson JT, Sun X, Dai H (2008) PEGylated nanographene oxide for delivery of water-insoluble cancer drugs. J Am Chem Soc 130:10876–10877
18. Kwon J, Lee SH, Park KH, Seo KH, Lee J, Kong BS, Kang K, Jeon S (2011) Simple preparation of high-quality grapheme flakes without oxidation using potassium salts. Small 7:864–868
19. Yamaguchi H, Eda G, Mattevi C, Kim H, Chhowalla M (2010) Highly uniform 300 mm wafer-scale deposition of single and multilayered chemically derived graphene thin films. ACS Nano 4:524–528
20. Kim KS, Zhao Y, Jang H, Lee SY, Kim JM, Kim KS, Ahn JH, Kim P, Choi JY, Hong BH (2009) Large-scale pattern growth of graphene films for stretchable transparent electrodes. Nature 457:706–710
21. Gomez De Arco L, Zhang Y, Schlenker CW, Ryu K, Thompson ME, Zhou CW (2010) Continuous, highly flexible, and transparent graphene films by chemical vapor deposition for organic photovoltaics. ACS Nano 4:2865–2873
22. Bae S, Kim H, Lee Y, Xu XF, Park JS, Zheng Y, Balakrishnan J, Lei T, Kim HR, Song YI, Kim YJ, Kim KS, Özyilmaz B, Ahn JH, Hong BH, Iijima S (2010) Roll-to-roll production of 30-inch graphene films for transparent electrodes. Nat Nanotechnol 5:574–578
23. Long D, Hong JY, Li W, Miyawaki J, Ling L, Mochida I, Yoon SH, Jang J (2011) Fabrication of uniform graphene discs via transversal cutting of carbon nanofibers. ACS Nano 5:6254–6261
24. Dresselhaus MS, Fung AWP, Rao AM, di Vittorio SL, Kuriyama K, Dresselhaus G, Endo M (1992) New characterization techniques for activated carbon fibers. Carbon 30:1065–1073
25. Kaneko K, Ishii C, Ruike M, Kuwubara H (1992) Origin of superhigh surface area and microcrystalline graphitic structures of activated carbons. Carbon 30:1075–1088
26. Oshida K, Kogiso K, Matsubayashi K, Kobayashi S, Endo M (1995) Analysis of pore structure of activated carbon fibers using high resolution transmission electron microscopy and image processing. J Mater Res 10:2507–2517
27. Prahas D, Kartika Y, Indraswati N, Ismadji S (2008) Activated carbon from jackfruit peel waste by H_3PO_4 chemical activation: pore structure and surface chemistry characterization. Chem Eng J 140:32–42
28. Girgis BS, El-Hendawy ANA (2002) Porosity development in activated carbons obtained from date pits under chemical activation with phosphoric acid. Micropor Mesopor Mat 52:105–117
29. Zuo S, Liu J, Yang J, Cai X (2009) Effects of the crystallinity of lignocellulosic material on the porosity of phosphoric acid-activated carbon. Carbon 47:3574–3584
30. Yu L, Tatsumi D, Zuo S, Morita M (2015) Promotion of crystal growth on biomass-based carbon using phosphoric acid treatments. BioResources 10:2406–2417
31. Kawano Y, Kondo T (2014) Preparation of aqueous carbon material suspensions by aqueous counter Collision. Chem Lett 43:483–485
32. Kondo T, Morita, M, Hayakawa, K, Onda Y (2008) Wet pulverizing of polysaccharides. U.S. Patent 7,357,339
33. Kondo T, Kose R, Naito H, Kasai W (2014) Aqueous counter collision using paired water jets as a novel means of preparing bio-nanofibers. Carbohydr Polym 112:184–290
34. Kose R, Mitani I, Kasai W, Kondo T (2011) "Nanocellulose" as a single nanofiber prepared from pellicle secreted by *Gluconacetobacter xylinus* using aqueous counter collision. Biomacromol 12:716–720

35. Tsuboi K, Yokota S, Kondo T (2014) Difference between bamboo- and wood-derived cellulose nanofibers prepared by the aqueous counter collision method. Nord Pulp Pap Res J 29:69–76
36. Rouquerol F, Rouquerol J, Sing KSW (1999) Adsorption by powders & Porous Solids. Academic Press, New York
37. Kaneko K, Ishii C, Ruike M, Kuwabara H (1992) Origin of superhigh surface area and microcrystalline graphitic structures of activated carbons. Carbon 30:1075–1088
38. Molina-Sabio M, Rodriguez-Reinoso F, Caturla F, Selles MJ (1995) Porosity in granular carbons activated with phosphoric acid. Carbon 33:1105–1113
39. Sing KSW (1985) Reporting physisorption data for gas/solid systems with special reference to the determination of surface area and porosity. Pure Appl Chem 57:603–619
40. Barrett EP, Joyner LG, Halenda PP (1951) The determination of pore volume and area distributions in porous substances. I. Computations from nitrogen isotherms. J Am Chem Soc 73:373–380
41. Marsh H, Rodríguez-Reinoso F (2006) Activated carbon (origins). In: Marsh H, Rodríguez-Reinoso F (eds) Activated carbon. Elsevier, Boston

Publisher's Note